Biallelic mutations in *MTPAP* associated with a lethal encephalopathy

Abstract

Background: A homozygous founder mutation in *MTPAP* / *TENT6*, encoding mitochondrial poly(A) polymerase, was first reported in six individuals of Old Order Amish descent demonstrating an early onset, progressive spastic ataxia with optic atrophy and learning difficulties. MTPAP contributes to the regulation of mitochondrial gene expression through the polyadenylation of mitochondrially-encoded mRNAs. Mitochondrial mRNAs with severely truncated poly(A) tails were observed in affected individuals, and mitochondrial protein expression was altered.

Objective: To determine the genetic basis of a perinatal encephalopathy associated with stereotyped neuroimaging and infantile death in three patients from two unrelated families.

Methods: Whole-exome sequencing was performed in two unrelated patients and the unaffected parents of one of these individuals. Variants and familial segregation were confirmed by Sanger sequencing. Polyadenylation of mitochondrial transcripts and *de novo* synthesis of mitochondrial proteins were assessed in patient fibroblasts.

Results: Compound heterozygous p.Ile428Thr and p.Arg523Trp substitutions in MTPAP were recorded in two affected siblings from one family, and a homozygous p.Ile385Phe missense variant identified in a further affected child from a second sibship. Mitochondrial poly(A) tail analysis demonstrated shorter post-transcriptional additions to the mitochondrial transcripts, as well as an altered expression of mitochondrial proteins in the fibroblasts of the two siblings compared to healthy controls.

Conclusion: Mutations in *MTPAP* likely cause an autosomal recessive perinatal encephalopathy with lethality in the first year of life.

Keywords:

MTPAP
Mitochondrial poly(A) polymerase
Encephalopathy
Leukoencephalopathy
Intracranial calcification

Introduction

A founder mutation in *MTPAP* (mitochondrial poly(A) RNA polymerase) was first reported in six individuals of Old Order Amish descent demonstrating an autosomal recessive spastic ataxia with optic atrophy and learning difficulties[1]. *In vitro*, this mutation reduced the ability of MTPAP to polyadenylate mitochondrial mRNA, a process shown to be involved in the stability and maturation of specific mitochondrial tRNAs[2,3] and the regulation of mitochondrial protein synthesis[3]. Thus, in individuals carrying the p.Asn478Asp mutation in the homozygous state, the poly(A) tails of mitochondrial mRNAs were severely truncated, and the expression of mitochondrial proteins was altered, accompanied by decreased activity of oxidative phosphorylation complexes I and IV[1,3]. A distinct cellular phenotype, characterized by increased DNA damage, reduced DNA repair kinetics and increased cell death following exposure to ionizing radiation, was described in two further individuals of Amish descent carrying the same homozygous *MTPAP* mutation, in the absence of features of clinical radiosensitivity[4].

Here, we report three patients exhibiting an early-onset, lethal encephalopathy in association with biallelic rare missense variants in *MTPAP*, functional evidence of reduced polyadenylation of mitochondrial transcripts, and altered expression of mitochondrial proteins in fibroblasts. These findings likely expand the disease spectrum associated with mutations in *MTPAP* to include a lethal encephalopathy.

Materials and methods

Standard Protocol Approvals, Registrations, and Patient Consents

The study was approved by the Leeds (East) Research Ethics Committee (reference number 10/H1307/132), the Prince of Wales Hospital Research Ethics Committee (SSA/13/HNE341) and the Comité de Protection des Personnes (ID-RCB/EUDRACT: 2014-A01017-40). Members of family F664 were consented for genomic testing under the institutional review board protocol AU/1/BA51117.

Molecular genetic investigations

DNA was extracted from whole blood samples using standard methods. Whole-exome sequencing was performed on genomic DNA from P1, P3 and the parents of P1. WES was performed in family F664 using an Ampliseq kit, with libraries analysed on a Life Technologies Proton instrument. P3 was sequenced using SureSelect Human All Exon kit (Agilent Technologies) for targeted enrichment and an Illumina HiSeq2000. Variants were assessed using the *in silico* programs CADD (https://cadd.gs.washington.edu), SIFT (http://sift.jcvi.org) and Polyphen2 (http://genetics.bwh.harvard.edu/pph2/), summarised in Varcards (http://varcards.biols.ac.cn), and population allele frequencies obtained from the ExAC (http://exac.broadinstitute.org) and gnomAD (http://gnomad.broadinstitute.org) databases. Sanger Sequencing was performed on DNA from all three patients and their parents to confirm the *MTPAP* variants found on exome sequencing. The reference sequence used for primer design and nucleotide numbering was *MTPAP* / *TENT6* (NM_018109.3). Primer sequences are available on request.

Investigation of mitochondrial function

Cell extracts were subjected to SDS-PAGE separation, transferred to nitrocellulose membrane and immunoblotted with primary antibodies against MTPAP (1D3, GTX70156, GeneTex) and the loading control cofilin (D3F9, #5175, Cell Signaling), followed by HRP-conjugated secondary antibodies (Invitrogen or Dako) and visualised using ECL blotting substrate (Bio-

Rad or GE Healthcare).

A modified mitochondrial poly(A) tail (MPAT) assay employed AlexaFluor® 647-labeled *RNA14*-specific nested forward primer 5′-AGT AAG CCT CTA CCT GCA CG-3′ (nt 9177–9196, accession: NC_012920.1) in combination with ANTI-LIGN primer 5′-GAC TGT GCA TGA TCT CAC-3′ in the second round of PCR[3]. The resulting products were separated on a 10% polyacrylamide/8.3M urea gel and directly imaged using a Typhoon FLA 9500 instrument (GE/Fujifilm).

Metabolic labelling of mitochondrial translation, to assess *de novo* mitochondrial protein synthesis, was performed essentially as described[5], with a modification of a 1 hour incubation with radiolabel. Cells were incubated with [^{35}S]-methionine/cysteine in the presence of the cytosolic translation inhibitor emetine dihydrochloride (100 µg/ml). Cell lysates (30µg) were separated by 15% (w/v) SDS-PAGE. Radiochemical signal was detected (Typhoon FLA 9500 instrument GE/Fujifilm) and proteins identified by comparing their migration patterns against established data[3,5,6]. Coomassie blue staining served as a loading control and the data were quantified using ImageQUANT TL (GE Healthcare).

Respiratory chain enzyme analysis was undertaken in patient fibroblasts as previously described[7].

Cellular assays of radiosensitivity

Fibroblasts were treated with 1 Gray (Gy) and collected at 1, 4 and 24 hours for assessment of 53BP1 foci. Cells were plated on coverslips, fixed with 2% paraformaldehyde, blocked in 1% BSA, permeabilized with 0.1% Triton X-100 (Sigma-Aldrich) and incubated with primary antibody against 53BP1 (1:200, Santa Cruz Biotechnology) for 1 hour at room temperature. The coverslips were washed and incubated with an AlexaFluor-488 secondary antibody (1:1000, Invitrogen) for 30 minutes at room temperature, and then mounted on slides using Vectashield containing DAPI (Vectorlabs). Foci were imaged using a LeicaSP8 40X oil immersion objective and Image Lab software. An average of 85 cells per individual were examined. The number of 53BP1 foci per nucleus were counted and presented as a mean and standard deviation. Experiments were repeated twice and a representative result is shown.

Measurements of cellular reactive oxygen species (ROS)

Carboxy-H2DCFDA (ThermoFisher Scientific) was used to assess the presence of cellular ROS levels. Fibroblasts were washed and incubated with PBS containing 10 mM Carboxy-H2DCFDA dye at 37°C for 30 minutes, and then either treated with 10 Gy, incubated with medium containing 10 mM H_2O_2 at 37°C for 2 hours, or sham treated. In each case samples were analysed within 10 minutes on a FLUOstar OPTIMA microplate reader (BMG labtech). Cellular ROS levels were presented as relative fluorescence units (RFU). Experiments were performed in triplicate, repeated twice and a representative result shown.

Structural modelling

Homology modelling of the human mitochondrial poly(A) polymerase was performed employing the Protein Data Bank (PDB) structure 3PQ1 as the template[8]. Both wild-type and I428T sequences were aligned with the template and modelled by means of SWISS-MODEL (Biozentrum, https://swissmodel.expasy.org/), using default parameters. Obtained PDB structures were visualised by PyMOL software (Open Source, Version 1.8.2.0).

Results

Clinical phenotype

Patient 1 (P1), a female, and patient 2 (P2), a male, were the first and second children of non-consanguineous parents of white European descent (family F664). The pregnancy with P1 was complicated by polyhydramnios, and antenatal ultrasound at 37 weeks gestation demonstrated mild bilateral ventriculomegaly. P1 was delivered at term weighing 2.94kg, with a head circumference of 33cms (9^{th} centile). She presented in the immediate post-natal period with respiratory distress necessitating oxygen supplementation for 10 days, and subsequently exhibited reduced tone, dystonic posturing and general irritability. Cerebrospinal fluid (CSF) examination on day 16 was blood-stained, with raised protein of 3.06g/L and minimally raised lactate of 3mmol/L (normal < 2.8). Repeat CSF examination on day 21 showed raised protein of 1.08g/L, a lactate of 1.8mmol/L (normal), and a leucocyte count of 8 cells/mm^3 and no erythrocytes. CSF amino acid profile was normal and cultures were sterile. Neopterin was not measured. TORCH screening and further infectious and metabolic testing was negative. A microarray analysis was normal, as was genetic testing of the seven genes known to be responsible for Aicardi-Goutières syndrome (AGS), and of the subunits of EIF2B (vanishing white matter disease). Neurological deterioration continued with spasmodic extensor posturing and stridor until death at 3.5 months of age. At this time her head circumference was 37cms (0.4^{th} – 2^{nd} centile). The next pregnancy, with P2, to the same couple was identified prenatally to have mild ventriculomegaly and polyhydramnios from 35 weeks gestation. Prenatal ultrasound and MRI at 28 and 34 weeks had not identified any significant white matter abnormality. P2 was delivered at 38 weeks gestation with normal birth weight and head circumference. Postnatal ultrasound and brain MRI on day 3 showed a similar appearance to that seen in his sister. Extensor posturing and stridor began from day 3 and he died at 6 weeks of age.

Patient 3 (P3: family F432), a male, was the fifth child of consanguineous parents of Pakistani descent. His four older sisters and a younger sibling are alive and well. He was delivered at term after a normal pregnancy weighing 2.75kg. In the immediate postnatal period he demonstrated reduced tone, stridor, feeding difficulties and failure to thrive. A tracheostomy was placed at age 2 months. At this time, ophthalmology and audiological review were normal. However, his head circumference was on the 0.4^{th} centile and he subsequently demonstrated severe psychomotor delay and became progressively dystonic with central hypotonia. Reflexes were diminished and electrophysiology was consistent with an axonal neuropathy. CSF examination at age 2 months revealed an increased number of lymphocytes (16/µl) and increased total neopterin (1074nmol/L, range 7 – 65nmol/L). Tetrahydrobiopterin and dihydrobiopterin were within normal limits. TORCH screening was negative. He died at the age of one year.

Brain imaging in all three individuals demonstrated diffusely increased signal on T2 weighted imaging in the cerebral white matter, and swelling of the frontal and anterior temporal white matter (Figure 1). There was cystic dilatation of the temporal horns of the lateral ventricles, and the cortex overlying the swollen white matter was stretched and smooth with frontal and perisylvian polymicrogyria. Susceptibility weighted imaging demonstrated multifocal areas of hypointensity representing mineralisation that is most likely to be calcification. Indeed, CT scanning in P3 at age 2 months demonstrated multiple foci of calcification in the white matter and basal ganglia bilaterally. Post mortem examination of P1 confirmed diffuse CNS white matter disease extending into the brainstem with absence of myelination, diffuse gliosis with a loose fibrillar, almost oedematous background and patchy macrophage collections. In addition, widespread focal calcification was confirmed microscopically, which appeared to arise in vessel adventitia. Nerves leaving the CNS were normally myelinated.

Genetic data and expression of MTPAP

Whole exome sequencing was performed using DNA from P1, P3 and the unaffected parents of P1. After filtering-out common polymorphisms, P1 was identified to be compound

heterozygous for the variants c.1283T>C (p.Ile428Thr) and c.1567C>T (p.Arg523Trp) in *MTPAP*, whilst P3 carried a homozygous c.1153A>T *MTPAP* transversion, leading to a p.Ile385Phe substitution. Sanger sequencing confirmed these data, also showing that P2 carried the same two substitutions as his sibling. Parental sequencing was consistent with biallelic inheritance in both families. None of these three variants is recorded on over 240,000 control alleles in the gnomAD database, and all are predicted to be deleterious by *in silico* analysis (Supplementary table 1). The combined annotation dependent depletion (CADD) score of all three variants was high, above the mutation significance cutoff (MSC) (Figure e1)[9,10]. The amino acid residues at positions 385, 428 and 523, all located in the fingers domain of MTPAP (Figure 1L), show a variable degree of conservation (Figure e2). Homology modelling performed on the most conserved variant I428T predicts a structural change around the helix at alpha12 (Figure e3). The p.Ile428Thr and p.Arg523Trp missense mutations do not interfere with normal expression of the MTPAP protein (Figure 1M). Since no cells were available from P3, the effect of the p.Ile385Phe mutation on MTPAP expression could not be determined.

Reduced polyadenylation of mitochondrial transcripts and altered expression of mitochondrial proteins

RNA14 encodes ATP8 and ATP6 as overlapping open reading frames in one of two bicistronic transcripts. Human *RNA14* is associated with the production of mtRNA demonstrating a poly(A) tail of 45 around nucleotides[11]. Compared to controls, cells from P1 and P2 showed a higher proportion of *RNA14* mRNA that was oligoadenylated or un-adenylated (Figure 2A). To assess the effect of altered mitochondrial transcript polyadenylation on mitochondrial protein expression, metabolic labelling of *de novo* synthesised mitochondrial proteins was performed in fibroblasts from these same patients (Figure 2B, C). When compared to controls and previously analysed material[3], the two patients studied here showed a similar pattern to reported MTPAP patients. The previous patient showed a modest decrease in the translation products of CytB (complex III), as well as in ND1 levels, with a slightly stronger decrease in COX2 and COX3 (complex IV)[3]. There was, however, no apparent change in the expression of a subset of complex I proteins (including ND3, ND4), the exception being ND5, which was clearly increased in both cases compared to controls. The latter finding may reflect the fact that under control conditions the *MTND5* transcript generally has only an oligo(A) rather than a poly(A) tail[11], and therefore might be relatively unaffected by a change in MTPAP activity. Quantification of the signals from P1 and P2, accounting for the loading according to the Coomassie blue staining, revealed a very similar effect on *de novo* synthesis (Figure 2C). Cells from P3 were unavailable for analysis.

Respiratory chain enzymes activities (CI, II, III and IV) assessed in fibroblasts from P1 and P2 were normal in both (Figure e4).

Radiosensitivity and ROS homeostasis

Staining for 53BP1-foci in fibroblasts of P1 and P2 after γ-irradiation showed no significant increase in either of the patients compared to controls (Figure e5A). Similarly, ROS production following γ-irradiation (Figure e5B) and H_2O_2 exposure (Figure e5C) was not statistically different between patient fibroblasts and cells from wild type individuals.

Discussion

Functional mitochondria underpin all cell metabolism through the production of ATP. This is efficiently achieved through oxidative phosphorylation that is carried out by five complexes embedded in the inner mitochondrial membrane. Four of these essential complexes are of dual genetic origin, with 13 of the constitutive polypeptides encoded by the mitochondrial genome[12]. Mitochondrially-encoded transcripts require maturation at the 3' end of the mt-mRNA[13], which

is performed by MTPAP[14]. The function of the poly(A) tail varies (reviewed in references 3 and 14). Yeast mt-mRNAs forgo any polyadenylation, whilst polyadenylation promotes transcript degradation in bacteria and plants. In human mitochondria the role of polyadenylation is complex, and incompletely understood. Experimental *in vitro* and cellular data clearly show that the presence and length of the poly(A) affects stability as well as translatability of the transcript[1,3,11,14,16,17]. In the absence of any adenylate addition, seven of the 13 mitochondrially-encoded transcripts would lack a stop codon, which directs protein-mediated release of the nascent peptide from the mitoribosome to allow integration into the relevant OXPHOS complex[11]. Since each of the 13 mtDNA-encoded proteins is essential, it is unsurprising that a defect in MTPAP activity could result in significant metabolic effects.

Autosomal recessive inheritance of a p.Asn478Asp missense *MTPAP* variant has previously been reported in only eight patients, all of whom were homozygous for the same Old Amish founder mutation[1,4]. Here we describe three further *MTPAP* missense variants in a further three individuals from two unrelated families, inherited either in the compound heterozygous or homozygous state, and provide evidence that these variants affect mitochondrial transcript polyadenylation and subsequent expression of mitochondrially encoded proteins. All three individuals demonstrated an encephalopathy leading to death in early infancy. Considering the overlap of clinical and neuroradiological features across these two new families, and the genetic and functional data that we present, we consider that these variants are likely pathogenic mutations. Similar to the previously reported mutation, the p.Ile428Thr and p.Arg523Trp missense substitutions do not interfere with MTPAP protein expression. However, we recorded a shared disturbance of mitochondrial transcript polyadenylation and mitochondrial protein expression. The fact that we did not observe an alteration of respiratory chain enzyme activity in fibroblasts from P1 and P2 suggests that MTPAP may have interactions / functions beyond those that are currently understood. Variation in severity of mitochondrial phenotypes in patients harbouring mutations in the same gene are not uncommon[18]. Additionally, analysis of fibroblasts from P1 and P2 did not recapitulate a cellular phenotype of increased DNA damage, reduced DNA repair kinetics and increased cell death following exposure to ionizing radiation recorded in two patients with the homozygous p.Asn478Asp MTPAP mutation[4]. The reason for this is unclear, but might perhaps relate to the use of different cell types.

Individuals of Old Order Amish descent carrying the previously described homozygous p.Asn478Asp MTPAP mutation demonstrated an early onset, progressive neurodegenerative condition with a decline in motor function and intellectual disability[1,4]. No neuroimaging data was reported for any of these individuals. The patients presented here exhibited a highly stereotyped clinic-radiological picture, characterised by a perinatal severe encephalopathy associated with neuroimaging somewhat reminiscent of congenital infection, profound developmental delay and death before the age of 1 year. The explanation for the observed variability in phenotypic expression remains unclear. Although all four mutations are located in close proximity to each other in the fingers domain of MTPAP, it is possible that substitutions of specific amino acids could lead to differential effects on MTPAP function. However, such an explanation is not obviously related to the effects on mitochondrial polyadenylation and protein expression recorded *in vitro*. The Old Order Amish genetically constitute a relatively homogenous population, so that the role of modifier genes might be relevant.

Thus, we report biallelic loss-of-function variants in *MTPAP* as a likely cause of an early-onset encephalopathy with lethality in infancy. As other mutations in *MTPAP* are identified, a fuller appreciation of the spectrum of clinical and cellular phenotypes associated with MTPAP dysfunction will be obtained, thereby better informing our understanding of the biological function of MTPAP.

Acknowledgments:

YJC acknowledges funding from the European Research Council (786142: Fellowship to Y.J.C) and a state subsidy managed by the National Research Agency (France) under the "Investments for the Future" (ANR-10-IAHU-01). ZMACL is funded by the Wellcome Centre for Mitochondrial Research (203105/Z/16/Z) and the EC Horizon 2020 Marie Curie-Sklodowska ITN REMIX. RWT is also funded by the Wellcome Centre for Mitochondrial Research (203105/Z/16/Z), as well as the MRC Centre for Neuromuscular Diseases (G0601943), the UK NIHR Biomedical Research Centre in Age and Age Related Diseases award to the Newcastle upon Tyne Hospitals NHS Foundation, the MRC/ESPRC Newcastle Molecular Pathology Node, the Lily Foundation and the UK NHS Highly Specialised Service for Rare Mitochondrial Disorders. LVE received funding from FWO-Vlaanderen. TAB acknowledges an NIHR Transitional Research Fellowship (TRF-2016-09-002)(with the views expressed those of the author and not necessarily those of the NHS, the NIHR or the Department of Health). YJC acknowledges Patrick Levy, Institut Imagine, Paris, for advice relating to the radiosensitivity assays. AR acknowledges Professor Marjo van der Knaap, Amsterdam, for initial review of the neuroimaging of family F664, and the parents of these children for their assistance with the study.

References

1. Crosby AH, Patel H, Chioza BA, et al. Chrzanowska-Lightowlers ZM, Cross HE, Lightowlers RN. Defective mitochondrial mRNA maturation is associated with spastic ataxia. Am J Hum Genet 2010;87:655-660.

2. Bratic A, Clemente P, Calvo-Garrido J, et al. Mitochondrial Polyadenylation Is a One-Step Process Required for mRNA Integrity and tRNA Maturation. PLoS Genet 2016;12:e1006028.

3. Wilson WC, Hornig-Do HT, Bruni F, et al. A human mitochondrial poly(A) polymerase mutation reveals the complexities of post-transcriptional mitochondrial gene expression. Hum Mol Genet 2014;23:6345-6355.

4. Martin NT, Nakamura K, Paila U, et al. Homozygous mutation of MTPAP causes cellular radiosensitivity and persistent DNA double-strand breaks. Cell Death Dis 2014;5:e1130.

5. Chomyn A. In vivo labeling and analysis of human mitochondrial translation products. Methods Enzymol 1996;264:197-211.

6. Hornig-Do HT, Montanari A, Rozanska A, et al. Human mitochondrial leucyl tRNA synthetase can suppress non cognate pathogenic mt-tRNA mutations. EMBO Mol Med 2014;6:183-193.

7. Kirby DM, Thorburn DR, Turnbull DM, Taylor RW. Biochemical assays of respiratory chain complex. Methods Cell Biol 2007;80:93-119.

8. Bai Y, Srivastava SK, Chang JH, Manley JL, Tong L. Structural basis for dimerization and activity of human PAPD1, a noncanonical poly(A) polymerase. Mol Cell 2011;41, 311-320.

9. Kircher M, Witten DM, Jain P, O'Roak BJ, Cooper GM, Shendure J. A general framework for estimating the relative pathogenicity of human genetic variants. Nat Genet 2014;46, 310-317.

10. Itan Y, Shang L, Boisson B, et al. The mutation significance cutoff (MSC): gene-level thresholds for variant-level predictions. Nat Methods 2016;13,109-110.

11. Temperley RJ, Wydro M, Lightowlers RN, Chrzanowska-Lightowlers ZM. Human mitochondrial mRNAs - like members of all families, similar but different. Biochim Biophys Acta 2010;1797:1081-1085.

12. Anderson S, Bankier AT, Barrell BG, et al. Sequence and organization of the human mitochondrial genome. Nature 1981;290:457-465.

13. Ojala D, Montoya J, Attardi G. tRNA punctuation model of RNA processing in human mitochondria. Nature 1981;290:470–474.

14. Tomecki R, Dmochowska A, Gewartowski K, Dziembowski A, Stepien PP. Identification of a novel human nuclear-encoded mitochondrial poly(A) polymerase. Nucl Acids Res 200;32:6001–6014.

15. Levy S, Schuster G. Polyadenylation and degradation of RNA in the mitochondria. Biochem Soc Trans 2016;44:1475-1482.

16. Nagaike T, Suzuki T, Katoh T, Ueda T. Human mitochondrial mRNAs are stabilized with polyadenylation regulated by mitochondria-specific poly(A) polymerase and polynucleotide phosphorylase. J Biol Chem 2005;280:19721–19727.

17. Slomovic S, Schuster G. Stable PNPase RNAi silencing: its effect on the processing and adenylation of human mitochondrial RNA. RNA 2008;14:310–323.

18. Imagawa E, Fattal-Valevski A, Eyal O, et al. Homozygous p.V116* mutation in C12orf65 results in Leigh syndrome. J Neurol Neurosurg Psychiatry 2016;87:212-216.

Figure legends

Figure 1: Neuroimaging features, protein schematic and western blot analysis.

MR images of P1 (A - D) at 3 weeks of age, P2 (E - G) at 4 days of age and P3 (H - K) at 7 weeks of age. Axial T2 weighted images (A - C, E - J) demonstrate diffusely increased signal in the cerebral white matter with swelling apparent in frontal (B, F, I) and anterior temporal (C, G, J) white matter. There is also cystic dilatation of the temporal horns of the lateral ventricles. Although the cortex overlying the swollen white matter is stretched and smooth there is also evidence of cortical malformation with frontal and perisylvian polymicrogyria. Susceptibility - weighted image (D) demonstrates multifocal areas of hypointensity representing mineralisation that is likely to be calcification. CT scan (K) demonstrates spot calcification in the deep cerebral white matter. Multiple low signal spots in the deep cerebral white matter on T2 images A and E are likely to represent calcification. L) Schematic of MTPAP depicting protein domains and their amino acid boundaries (NTD, N-terminal domain). All disease-associated mutations are located in the fingers domain, within or close to the poly(A) polymerase domain and / or the active site cleft. The p.Asn478Asp (N478D) Amish founder mutation is shown in red. (M) Mitochondrial poly(A) polymerase (MTPAP) expression in fibroblast cell extracts from P1 and P2 detected by western blot, with cofilin used as a loading control.

Figure 1

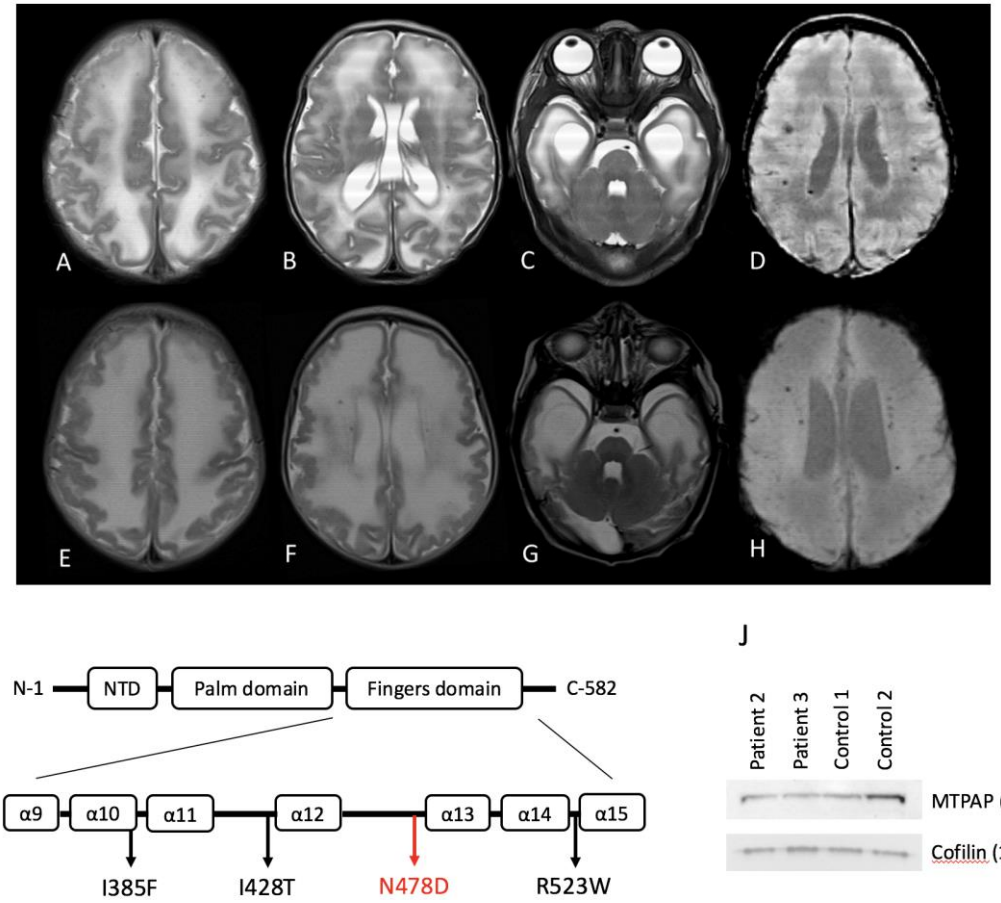

Figure 2: Analysis of mitochondrial poly(A) tail length and proteins.

(A) Mitochondrial poly(A) tail length of *RNA14* in fibroblasts from P1, P2 and a healthy control. Positions of full length, short, or oligoadenylated mRNA are shown relative to the size markers (on the left). Compared to control, cells from P1 and P2 showed a higher proportion of *RNA14* mRNA that was oligoadenylated or un-adenylated. (B) To assess the expression of mitochondrial proteins, ^{35}S metabolic labelling of mitochondrial proteins was performed using fibroblasts from P1, P2 and two healthy controls. Coomassie blue staining (CBS) served as a loading control and the data were quantified using ImageQuant TL (GE Healthcare). (C) A modest decrease was observed in the translation products COX2 and COX3 (complex IV). *De novo* synthesis of ND5, ND6 and ND3 was clearly increased in both cases compared to controls.

Figure 2